Atomic layer deposition of Nb-doped ZnO for thin film transistors

A. Shaw, J. S. Wrench, J. D. Jin, T. J. Whittles, I. Z. Mitrovic, M. Raja, V. R. Dhanak, P. R. Chalker, and S. Hall

Atomic layer deposition of Nb-doped ZnO for thin film transistors

A. Shaw,[1] J. S. Wrench,[2] J. D. Jin,[1] T. J. Whittles,[3] I. Z. Mitrovic,[1] M. Raja,[1] V. R. Dhanak,[3] P. R. Chalker,[2] and S. Hall[1,a)]

[1]*Department of Electrical and Electronic Engineering, University of Liverpool, Liverpool L69 3GJ, United Kingdom*
[2]*School of Engineering, Centre for Materials and Structures, University of Liverpool, Liverpool L69 3GH, United Kingdom*
[3]*Department of Physics and Stephenson Institute of Renewable Energy, University of Liverpool, Liverpool L69 3BX, United Kingdom*

We present physical and electrical characterization of niobium-doped zinc oxide (NbZnO) for thin film transistor (TFT) applications. The NbZnO films were deposited using atomic layer deposition. X-ray diffraction measurements indicate that the crystallinity of the NbZnO films reduces with an increase in the Nb content and lower deposition temperature. It was confirmed using X-ray photoelectron spectroscopy that Nb^{5+} is present within the NbZnO matrix. Furthermore, photoluminescence indicates that the band gap of the ZnO increases with a higher Nb content, which is explained by the Burstein-Moss effect. For TFT applications, a growth temperature of 175 °C for 3.8% NbZnO provided the best TFT characteristics with a saturation mobility of 7.9 cm^2/Vs, the current On/Off ratio of 1×10^8, and the subthreshold swing of 0.34 V/decade. The transport is seen to follow a multiple-trap and release mechanism at lower gate voltages and percolation thereafter. *Published by AIP Publishing.* [http://dx.doi.org/10.1063/1.4968194]

Zinc oxide (ZnO) has received a great deal of attention over the recent years particularly for the application of transparent electronics for active matrix displays. ZnO shows advantages when compared to materials such as amorphous silicon in terms of higher saturation mobilities[1,2] and a larger band gap (Eg ~ 3.37 eV)[1] enabling the potential for transparent display technology. The atomic layer deposition (ALD) of ZnO provides the potential for large area homogeneous films. Low temperature ALD (<150 °C) is known to achieve the best performance as the films are less conductive, with the reported mobilities of >10 cm^2/Vs.[3–5] However, indium gallium zinc oxide (IGZO) is the preferred ZnO based material for thin film transistors (TFTs)[6] due to its relatively high electron mobility, stability, and good control of conductivity.

However, for large scale production, non-indium based materials are desirable for cost effectiveness, hence the requirement for alternative dopants. Research into non-indium based ZnO materials for TFT application includes: gallium,[7] silicon,[8] and magnesium.[9] These dopants act as effective oxygen vacancy (V_o) suppressors and can further increase the band-gap of the ZnO through the Burstein-Moss effect.[7–9] Niobium (Nb) has the potential as a dopant, due to its high valency (Nb^{5+}) which offers the prospect of a V_o suppressor, superior to the dopants gallium (Ga^{3+}), silicon (Si^{4+}), and magnesium (Mg^{2+}). Furthermore, Nb can act as an effective substitutional dopant for Zn^{2+} and subsequently reduce the disorder and carrier scattering. To date, the studies of Nb-doped ZnO (NbZnO) films have been reported using pulse layer deposition (PLD) [10,11] and sputtering.[12] The use of Nb-doping in transparent semiconducting oxides has been reported for TiO$_x$ TFTs.[13] In this letter, we present the physical and electrical characteristics of NbZnO films for active layers in TFT applications.

The NbZnO films of nominal thickness 50 nm were deposited using ALD on heavily doped, thermally oxidized (50 nm) n-type Si wafers. A capping layer of 5 nm Al$_2$O$_3$ was first deposited by ALD at 200 °C on the SiO$_2$. The active layer NbZnO was then deposited at 200 °C using the precursors diethlyzinc (DEZn) and niobium pentaethoxide (Nb(OEt)$_5$); temperatures of these precursors entering the chamber were ambient and 140 °C, respectively. The Nb ALD cycle fraction was varied from 1% to 12.5%, where the NbZnO films were made by first depositing the x-cycles of ZnO by successive steps of DEZn and then H$_2$O vapor on the surface. After the x-cycles of ZnO, a single Nb$_2$O$_5$ cycle is deposited by the successive steps of Nb(OEt)$_5$ and H$_2$O. The process is repeated until the desired film thickness is reached. For example, a film with a Nb cycle percentage of 2% would be achieved by 49 cycles of DEZn and H$_2$O (x = 49) followed by 1 cycle of Nb(OEt)$_5$ and H$_2$O repeated 6 times giving a total of 294 ZnO and 6 Nb$_2$O$_5$ cycles. This equates to a cycle fraction of 0.02 and a cycle percentage of 2% ($6/(294+6) \times 100\% = 2\%$). The thickness of the films was confirmed by spectroscopic ellipsometry as 52 ± 2 nm. The effect of the ALD growth temperature was tested for 3.8% NbZnO at 150, 175, 200, and 225 °C.

X-ray diffraction (XRD), photoluminescence (PL), and X-ray photoelectron spectroscopy (XPS) were performed to determine the crystallographic nature, optical properties, and composition, respectively. The XRD measurements were performed on 1% NbZnO as-deposited, 1% to 12.5% NbZnO annealed for 1 hour at 300 °C air, and 3.8% NbZnO grown at 150 °C, 200 °C, and 225 °C annealed under the same conditions. The crystalline phases were identified by XRD using Cu Kα radiation (0.154051 nm, 40 kV, and 50 mA), and the

a)Author to whom correspondence should be addressed. Electronic mail: S.Hall@liverpool.ac.uk
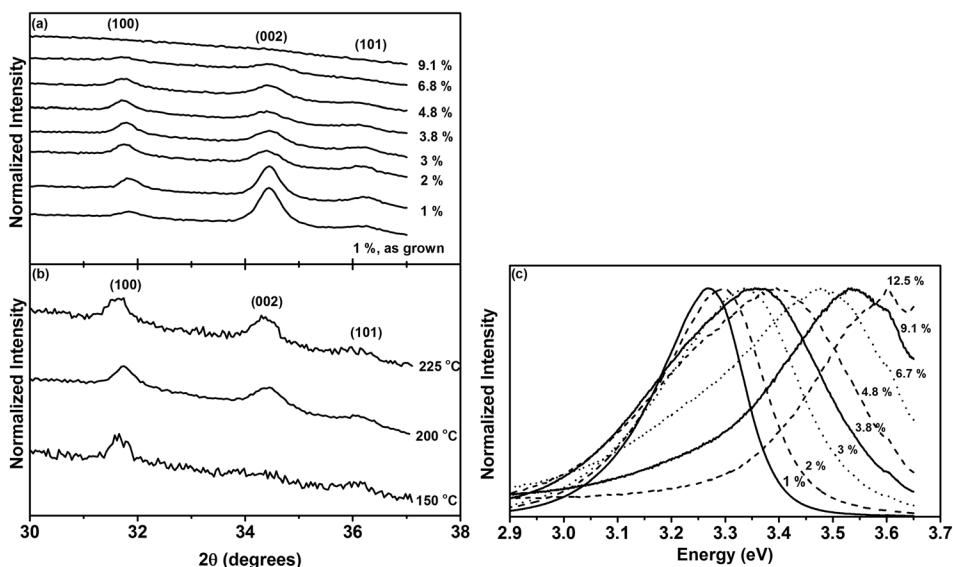
FIG. 1. Physical characterization for NbZnO films (a) XRD for different Nb cycle percentages annealed at 300 °C and 1% NbZnO as grown at 200 °C, (b) XRD of 3.8% NbZnO grown at different temperatures, and (c) PL of NbZnO with an increase in the Nb content.

diffraction patterns are shown in Figs. 1(a) and 1(b). The films are polycrystalline with peaks (100), (002), and (101). Fig. 1(a) shows the comparison between a 1% NbZnO film as-grown at 200 °C and after annealing. The act of annealing in air enhances the film crystallinity as indicated by the increase in the intensity of the (100) and (101) peaks as well as the reduction of their full width at half maxima (FWHM) from 0.50 to 0.45 and 0.51 to 0.44, respectively. In general, there is greater (002) directionality, although as the Nb content is increased, the films' crystallinity is reduced eventually becoming amorphous at 9.1% and above. For the (002) peak, the grain size is reduced from 20 to 14 nm and an increase in Nb from 1% to 6.8% is calculated using the Scherrer equation.[14] This reduction in ZnO crystallinity with Nb concentration has also been reported when grown using PLD.[11] Fig. 1(b) demonstrates that reducing the growth temperature serves to reduce the crystallinity of the ZnO as there are no observable (002) or (101) peaks at 150 °C.

The PL measurements were performed using a 325 nm (3.82 eV) He-Cd laser and a Raman confocal microscope set to 100 μm aperture coupled to a single grating spectrometer equipped with a notch filter and a CCD camera detector. The PL spectrum of the as-deposited samples with varying Nb content is shown in Fig. 1(c). As the Nb cycle percentage is increased, the band edge increases to 3.58 eV, consistent with spectroscopic ellipsometry results.[15] This increase can be

described by the Burstein-Moss effect; similar band energy shifts have been reported for NbZnO prepared by PLD,[11] spray pyrolysis,[16] and electrostatic spray deposition.[17]

The core level (CL) structure and the occupied density of states in the valence band were probed by XPS; further experimental details of which can be found elsewhere.[18] For the XPS measurements, 10 nm films were used, which correspond to the nominal surface sensitivity of the technique. Core level peak energies were corrected using adventitious carbon C 1s peak at 284.6 eV for all samples. The CL spectra for the Nb $3d_{5/2}$ and Zn $2p_{3/2}$, O 1s for bulk ZnO, 3.8% and 12.5% NbZnO grown at 200 °C are shown in Fig. 2. Fig. 2(a) shows that the Nb $3d_{5/2}$ peak for bulk Nb_2O_5 has a binding energy (BE) of 207.1 eV indicating the presence of Nb^{5+}.[19] For 3.8% and 12.5% NbZnO, the Nb $3d_{5/2}$ peak shifts to a lower BE of 206.8 eV. Conversely, Fig. 2(b) indicates an increase in the BE for the Zn $2p_{3/2}$ peak, from 1020.1 eV for bulk ZnO to 1021.2 eV and 1021.3 eV for 3.8% and 12.5% NbZnO, respectively. This implies that Nb^{5+} species are present in the film as a substitutional dopant due to the nature of the charge transfer. Fig. 2(c) indicates that for bulk ZnO, the O 1s CL shows 3 sub-peaks relating to (i) the oxygen atoms bonded with the nearest neighbor metal ion species (Zn-O), (ii) the oxygen atoms in the vicinity of an oxygen vacancy (labelled as O^{2-} deficiency peak), and (iii) surface oxygen such as O-C-O or hydroxyl groups.[19] Furthermore, 3.8 and
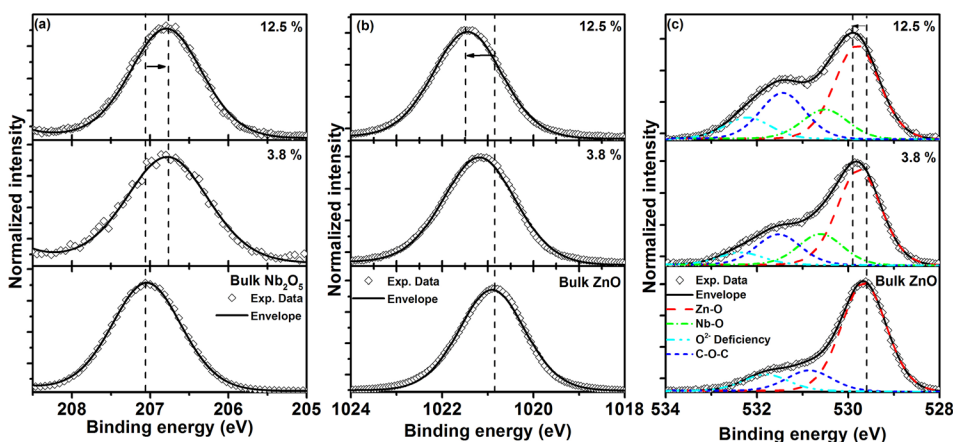
FIG. 2. XPS fittings of (a) Nb $3d_{5/2}$ core level for bulk Nb_2O_5, 3.8% NbZnO and 12.5% NbZnO (b) Zn $2p_{3/2}$ core level for bulk ZnO, 3.8% NbZnO and 12.5% NbZnO and (c) O 1s core level for bulk ZnO, 3.8% NbZnO and 12.5% NbZnO.

TABLE I. TFT characteristics for the 3.8% NbZnO growth temperature study and comparison with pure ZnO and 12.5% NbZnO showing the average of 5 measured devices.

Nb cycle (%)	Temp. (°C)	On/Off ratio	V_T (V)	μ_{sat} (cm²/Vs)	SS (mV/dec)	V_{FB} (V)	T_o (K)
0[15]	200	1×10^4	9.3 ± 1.0	1.4 ± 0.2	2970 ± 300	…	…
3.8	150	3×10^8	7.9 ± 0.2	4.8 ± 0.1	220 ± 20	-4.0	539
	175	1×10^8	8.5 ± 0.1	7.9 ± 0.1	340 ± 40	-1.5	541
	200	1×10^7	9.3 ± 0.1	7.9 ± 0.1	470 ± 30	-3.3	570
	225	9×10^6	9.8 ± 0.1	7.0 ± 0.1	870 ± 20	-1.2	620
12.5[15]	200	1×10^7	1.0 ± 1.0	0.1 ± 0.1	1080 ± 200	…	…

12.5% NbZnO has these sub-peaks with the addition of a sub-peak with a BE of 530.5 eV, which we assign to the presence of an Nb-O environment confirmed by the O 1s Nb_2O_5 peak (see supplementary material). It is evident that the O 1s CL shifts to higher binding energies with the addition of Nb from 529.5 eV to 529.9 eV as a consequence of Nb^{5+} species present within the film. Furthermore, it is evident that there is an increase of O^{2-} deficiencies with an increase in Nb^{5+}, shown by the increased sub-peak at 531.4 eV.[20,21] Moreover, from the XRD spectra in Fig. 1(a), increasing Nb doping concentration serves to reduce the film crystallinity, potentially creating more dangling bonds, hence the higher ratio of O^{2-} deficiency sub-peak for 12.5% NbZnO. Subsequently, the oxygen vacancies can be reduced by annealing in an oxygen rich environment (see supplementary material). The high binding energy sub-peak likely to be due to O-C-O, experiences a slight increase with the Nb content, presumably related to carbon residue from the ALD process. It is worth noting that the percentage of Nb within the films was estimated to be 4% and 14% for the 3.8% and 12.5% NbZnO, respectively, demonstrating that for ALD NbZnO, Nb doping does not hinder the growth of the ZnO.

TFTs were fabricated using 3.8% NbZnO, deposited at 150, 175, 200, and 225 °C. The aluminum source/drain contacts were thermal evaporated and patterned using photolithography. The channel length (L) and width (W) are 40 μm and 400 μm, respectively. Finally, the TFTs were annealed in air for 1 h to further reduce the film conductivity. It is the conventional practice to utilize the ideal MOSFET equation extract key parameters to enable an effective comparison of results in the literature

$$I_{DS} = \frac{W}{2L} C_{ox} \mu_{sat} (V_{GS} - V_T)^2 \text{ for } V_{DS} > V_{GS} - V_T, \quad (1)$$

where C_{ox} is the gate capacitance per unit area, μ_{sat} is the effective saturation mobility, V_{GS}, V_T, and V_{DS} are the gate, threshold, and drain voltages, respectively. The subthreshold swing (SS) is defined in the usual manner, as $(\log(I_{DS})/V_{GS})^{-1}$.

Table I shows the extracted parameters for different growth temperatures, together with pure ZnO and 12.5% NbZnO for the purpose of comparison. Typical TFT output and transfer characteristics are shown in Figs. 3(a) and 3(b), respectively, for the 3.8% NbZnO film grown at 175 °C, where the symbols designate measured characteristics.

Comparing the different Nb cycle percentages in Table I, it is evident that Nb serves to increase the On/Off ratio by reducing the off-current.[15] The On/Off ratio is defined as the maximum current and when the TFT begins to conduct.

Moreover, small Nb cycle percentages serve to increase the on-current; however, the increased Nb concentration reduces the films' conductivity, indicated by the change in μ_{sat}.[15] The improved μ_{sat} is considered to be due to the high oxidation state of Nb^{5+}. Table I indicates that the On/Off ratio decreases with an increase ingrowth temperature for 3.8% NbZnO, together with a positive shift in V_T. Furthermore, μ_{sat} stays about the same for temperatures above 175 °C. The lower mobility for 150 °C NbZnO can be attributed to the reduced crystallinity apparent from Fig. 1(b). Conversely, SS is improved for the lower temperature grown NbZnO, implying a better interface between Al_2O_3 and NbZnO. It is evident from Table I that the 175 °C NbZnO TFT has the best characteristics with On/Off ratio $= 1 \times 10^8$, $\mu_{sat} = 7.9$ cm²/Vs, and $SS = 340$ mV/dec.

More appropriate physical modelling of the TFTs is achieved by considering a power law dependency of current on gate voltage, which arises by considering an exponential density of electron states (DoS) in the material.[22] The drain current mechanism is then described by the multi-trapping and release (MTR) model

$$I_{DS} = \frac{W}{L} \beta \left[\left(V_{GS} - V_{FB} - (I_{DS}R_S) \right)^\gamma - \left(V_{GS} - V_{FB} - (I_{DS}R_D) \right)^\gamma \right]. \quad (2)$$

The power law index is defined as $\gamma = T_o/T$, where T_o is a characteristic temperature related to the exponential DoS,[22] V_{FB} is the flat band voltage, β is a transconductance parameter,
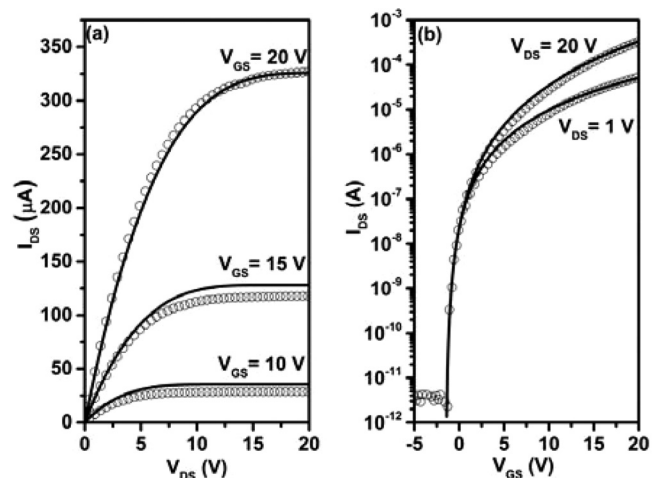
FIG. 3. (a) Output characteristics and (b) transfer characteristics for $V_{DS} = 1$ V and $V_{DS} = 20$ V of 175 °C grown 3.8% NbZnO TFTs. The solid line shows the fitted theory of Eq. (2).

and R_S and R_D are the source and drain series resistances, respectively. Fitting of (2) with experimental data was performed by linear regression with a regression coefficient, R^2 of 0.99 and 0.93 for the transfer and output characteristics, respectively. Fits for the 175 °C NbZnO TFT are shown in Fig. 3. The power dependency of I_{DS} increased from 3.6 to 4.13 with temperature and the corresponding T_o, as shown in Table I. It can be seen that T_o and SS are correlated and is representative of the degree of disorder in the film, which translates into a poorer SS. Comparing the TFT performance with our similar work on Mg doping,[23] the lower T_o and SS indicate that Nb is a more effective dopant for ZnO. Furthermore, it has been reported for metal oxide semiconductors that for sufficiently large V_{GS}, a mechanism of percolation dominates the current transport.[24,25] Following the analysis outlined in Refs. 24 and 25, the TFTs are seen to follow a similar transport physics with the onset of percolation current ($E_F = E_C$) at $V_{GS} \approx 15\,V$ for 175 °C NbZnO. The associated effective density of tail states was found to be $1.5 \times 10^{18}\,cm^{-3}$.

In conclusion, ALD has been used to deposit NbZnO films for TFT applications. It has been established from XPS that Nb^{5+} exists within the NbZnO matrix. Furthermore, XRD indicates that NbZnO films are polycrystalline with low Nb cycle percentages over a range of growth temperatures. However, as the Nb cycle percentage increases, the films become amorphous while shifting the band gap to higher energies. Optimum TFT performance was achieved with 175 °C 3.8% NbZnO where the μ_{sat} is superior to ALD ZnO doped with Mg[9] and Si.[8]

See supplementary material for XPS CL spectra of bulk Nb_2O_5 O 1s and the effects of annealing in air on 12.5% NbZnO O 1s.

[1] E. Fortunato, P. Barquinha, and R. Martins, Adv. Mater. **24**, 2945 (2012).

[2] C. Brox-Nilsen, J. Jin, Y. Luo, P. Bao, and A. M. Song, IEEE Trans. Electron Devices **60**, 3424 (2013).

[3] P. K. Nayak, Z. Wang, and H. N. Alshareef, Adv. Mater. **28**, 7736 (2016).

[4] Y. Y. Lin, C. C. Hsu, M. H. Tseng, J. J. Shyue, and F. Y. Tsai, ACS Appl. Mater. Interfaces **7**, 22610 (2015).

[5] Y. H. Wang, Q. Ma, L. L. Zheng, W. J. Liu, S. J. Ding, H. L. Lu, and D. W. Zhang, IEEE Trans. Electron Devices **63**, 1893 (2016).

[6] H. Hosono, J. Non-Cryst. Solids **352**, 851 (2006).

[7] W. J. Park, H. S. Shin, B. D. Ahn, G. H. Kim, S. M. Lee, K. H. Kim, and H. J. Kim, Appl. Phys. Lett. **93**, 083508 (2008).

[8] S. H. Lee, K. W. Cha, and J. S. Park, Thin Solid Films **596**, 72 (2015).

[9] J. S. Wrench, I. F. Brunell, P. R. Chalker, J. D. Jin, A. Shaw, I. Z. Mitrovic, and S. Hall, Appl. Phys. Lett. **105**, 202109 (2014).

[10] J. M. Lin, Y. Z. Zhang, Z. Z. Ye, X. Q. Gu, X. H. Pan, Y. F. Yang, J. G. Lu, H. P. He, and B. H. Zhao, Appl. Surf. Sci. **255**, 6460 (2009).

[11] J. Shao, W. Dong, D. Li, R. Tao, Z. Deng, T. Wang, G. Meng, S. Zhou, and X. Fang, Thin Solid Films **518**, 5288 (2010).

[12] F. Cao, Y. D. Wang, D. L. Liu, J. Z. Yin, B. J. Guo, L. Li, and Y. P. An, Chin. Phys. Lett. **26**, 034210 (2009).

[13] K. C. Ok, J. Park, J. H. Lee, B. D. Ahn, J. H. Lee, K. B. Chung, and J. S. Park, Appl. Phys. Lett. **100**, 142103 (2012).

[14] A. L. Patterson, Phys. Rev. **56**, 978 (1939).

[15] A. Shaw, J. D. Jin, I. Z. Mitrovic, S. Hall, J. S. Wrench, and P. R. Chalker, in *2016 Joint International EUROSOI Workshop and International Conference on Ultimate Integration on Silicon (EUROSOI-ULIS), Vienna, Austria, 25–27 January 2016* (IEEE, New York, 2016), p. 28.

[16] V. Gokulakrishnan, S. Parthiban, K. Jeganathan, and K. Ramamurthi, J. Electron. Mater. **40**, 2382 (2011).

[17] H. Yoon, B. N. Joshi, S.-H. Na, J.-Y. Choi, and S. S. Yoon, Ceram. Int. **40**, 7567 (2014).

[18] T. J. Whittles, L. A. Burton, J. M. Skelton, A. Walsh, T. D. Veal, and V. R. Dhanak, Chem. Mater. **28**, 3718 (2016).

[19] M. K. Bahl, J. Phys. Chem. Solids **36**, 485 (1975).

[20] P. T. Hsieh, Y. C. Chen, K. S. Kao, and C. M. Wang, Appl. Phys. A **90**, 317 (2008).

[21] Y. Jung, W. Yang, C. Y. Koo, K. Song, and J. Moon, J. Mater. Chem. **22**, 5390 (2012).

[22] F. Torricelli, J. R. Meijboom, E. Smits, A. K. Tripathi, M. Ferroni, S. Federici, G. H. Gelinck, L. Colalongo, Z. M. Kovacs-Vajna, D. de Leeuw, and E. Cantatore, IEEE Trans. Electron Devices **58**, 2610 (2011).

[23] A. Shaw, T. J. Whittles, I. Z. Mitrovic, J. D. Jin, J. S. Wrench, D. Hesp, V. R. Dhanak, P. R. Chalker, and S. Hall, in *European Solid-State Device Research Conference, Graz, Austria, 14–18 September 2015* (IEEE, New York, 2015), p. 206.

[24] S. Lee, K. Ghaffarzadeh, A. Nathan, J. Robertson, S. Jeon, C. Kim, I. H. Song, and U. I. Chung, Appl. Phys. Lett. **98**, 203508 (2011).

[25] M. Ghittorelli, F. Torricelli, and Z. M. Kovács-Vajna, IEEE Electron Device Lett. **36**, 1340 (2015).